Shape Effects in Random Sequential Adsorption of Zero-Area Angled Objects on a Continuum Substrate

M. D. Khandkar* and A. V. Limaye†
Department of Physics, University of Pune, Pune 411 007, India

S. B. Ogale‡
Department of Physics, University of Maryland, College Park, Maryland 20742
(Received 26 July 1999)

Random sequential adsorption (RSA) of zero-area symmetric angled objects on a continuum substrate is studied for the full range (0°–180°) of values of the arm angle ϕ. The value of exponent α [in $\rho(t) \sim t^{\alpha}$, where $\rho(t)$ is the number density] exhibits a dramatic crossover feature near $\phi = 0°$ or 180°. It is shown that the functional dependence of α on ϕ is governed by the degree of shape dependent frustration of the adsorption process. The crucial role of the geometrical character of the zero-area object in RSA dynamics is thus established.

PACS numbers: 82.20.Mj, 05.70.Ln, 68.10.Jy

Over the past decade considerable scientific effort has been devoted to the understanding of the random sequential adsorption (RSA) process, in view of its known significance in the context of a wide variety of deposition processes involving species ranging from pointlike particles to proteinlike complex structures in physical, chemical, and biological systems [1]. In RSA, objects are sequentially dropped on a substrate at random and get rigidly adsorbed if they do not overlap with the previously adsorbed objects. The RSA models are broadly classified into continuum models and lattice models on the basis of the nature of the substrate. They are also characterized by the type of the objects, either of nonzero (finite) area or of zero area.

In the case of objects with nonzero (finite) area, the already adsorbed objects cause blocking of the area available for new additions, which limits the value of coverage $\theta(t)$, the fraction of the total substrate area covered by the adsorbed objects at instant t. This limit, $\theta(\infty)$, is the jamming limit, and the approach to $\theta(\infty)$ is a matter of considerable interest. Swendsen [2] presented an argument that RSA of d-dimensional hard spheres should follow the law, $\theta(\infty) - \theta(t) \sim t^{-p}$, where $p = 1/d$, which agreed with the simulation results for hard disks by Feder [3]. However, for unoriented squares, Tarjus and Viot [4] found that the exponent $p \neq 1/d$, but is equal to $1/n$, "n" being the number of degrees of freedom per object. Noticing that weakly elongated ellipses also follow the same behavior, they suggested universality of this behavior. However, for anisotropic objects like ellipses, the geometrical properties such as shape and elongation are also quite influential for the value of exponent "p" [5].

Viot *et al.* [6] have studied RSA of rectangles with aspect ratio β and have observed that $\theta_{\beta}(\infty) \to 0$ as $\beta \to \infty$, as expected. By studying the RSA of line segments on 2D continuous substrate, Sherwood [7] suggested that the number density $\rho(t) \sim t^{\alpha}$ with $\alpha = \frac{1}{3}$, implying a relation $\alpha = 1/n$. His simulations substantiated these findings. However, Ziff and Vigil [8] showed that at longer times, the exponent $\alpha \approx 0.38$. Later, by studying a 1D system, Tarjus and Viot [9] showed that the exponents describing the RSA of objects with and without proper finite area are not simply related, and analytically obtained a nontrivial, irrational exponent $\alpha = \sqrt{2} - 1$.

To the best of our knowledge, however, there are no reports on the RSA of zero-area objects of shapes other than the line segments on continuum, in spite of the known fact that the shape of the object does play a significant role in the case of the kinetics of RSA of nonzero area objects. In order to probe this issue we have performed a simulation experiment wherein we have studied the RSA of "symmetric (equal arm lengths) angled objects" of zero area on a 2D continuous substrate. Though the object is an angled one, being symmetric it has the same number of degrees of freedom (i.e., three) as those for a line segment. Such studies should be relevant for the case of adsorption of molecules with noncollinear bonds.

We consider a 2D continuous substrate of size $L \times L$, and symmetric angled objects of arm length l are dropped randomly on it with random orientations. l is kept equal to $L/20$ in order to minimize the finite size effects. The runs were also carried out for $l = L/10$ and $l = L/50$ to check for the size dependence, and no significant dependence was observed for the sizes studied. The simulations were carried out for various values of angle ϕ between the two arms, the objects being termed as "angled objects." For $\phi = 0°$ and 180° the objects are linear (collinear arms), and henceforth will be termed as needles. The time t is counted as the number of total attempts including both the successful and the failed ones. In each case, the RSA process was observed for the time up to $t = 10^8$ units and 5 runs of simulations were carried out for each type of object. An average time for a single run is about 8 hours of HP(735/125) workstation.

Figure 1 gives the number density $\rho(t)$ plotted against time t on log-log scale, for a few representative values

 0031-9007/00/84(3)/570(4)$15.00

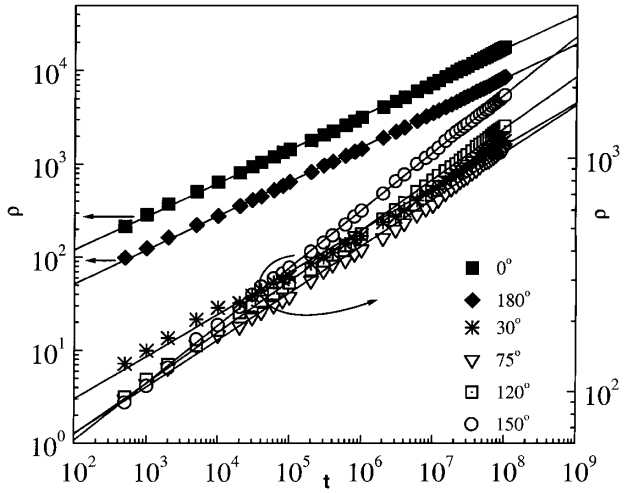

FIG. 1. Plot of number density $\rho(t)$ against time t on log-log scale for different object angles ϕ. The arrows indicate that the graphs corresponding to $\phi = 0°$ and $\phi = 180°$ refer to the ρ axis on the left-hand side. Remaining ones (indicated together by a curved arrow) refer to the ρ axis on the right-hand side.

of object angle ϕ. A marked difference between RSA of needles and that of angled objects can be immediately noticed. After long enough time, at any instant t, the adsorption rate for needles is far more than that for the angled objects. However, in both cases the relation $\rho(t) \sim t^{\alpha}$ is followed in the asymptotic time regime.

The dependence of α on ϕ is plotted in Fig. 2. The value of α is 0.369 ± 0.011 for the objects with $\phi = 0°$ and 0.379 ± 0.004 for $\phi = 180°$, and is in good agreement with earlier works [8,10]. However, the most striking feature is that a very small change in the angle ϕ away from 0° or 180° brings about a dramatic drop in the value of the exponent α; e.g., when ϕ changes from 0° to 1°, the average value of α drops from 0.369 to 0.188. The drop near 180°, although equally dramatic, is smaller in magnitude. It is important to emphasize that even a small departure from $\phi = 0°$ or 180° causes a crossover from collinearity to noncollinearity, the noncollinear object being capable of two-dimensional or areal blocking. The dramatic drop in α for angled objects is thus a clear consequence of the enhanced frustration of the spatial adsorption. Interestingly, away from the crossover regime, say from $\phi \sim 30°$ to $\phi \sim 150°$, the value of α increases gradually with increase in the value of ϕ. We will deal with this interesting aspect after we analyze the primary difference in the adsorption systematics for needles and angled objects.

In the case of the RSA of needles, the configuration formed in the long time regime is made up of a large number of microdomains. Any such domain contains a very large number of needles all very close to each other and nearly parallel. Both Sherwood [7] and Tarjus and Viot [9] have considered the growth within a single ordered domain and obtained $\alpha = \frac{1}{3}$ and $\alpha = \sqrt{2} - 1$, respectively. In the asymptotic regime, most new additions are inside the domains only, and a vanishingly small number of additions

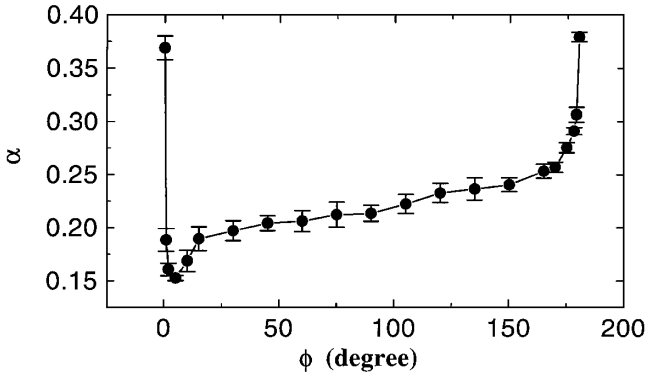

FIG. 2. Plot showing ϕ dependence of α.

take place if newly arriving objects are to be positioned in the interdomain spaces. The exponent is thus expected to get lowered when one considers a growth on the substrate as a whole, rather than in a single domain. Clearly, the sizes of domains have significant influence on the kinetics of RSA in this late phase of adsorption.

In Figs. 3(a) and 3(b) we compare the geometric status of the representative cases of needle and angled object adsorption, for the same total length of either object. Interestingly, the mesh structure of the open spaces does not appear too different for the eye, but it should look very different for further adsorbing objects depending on whether

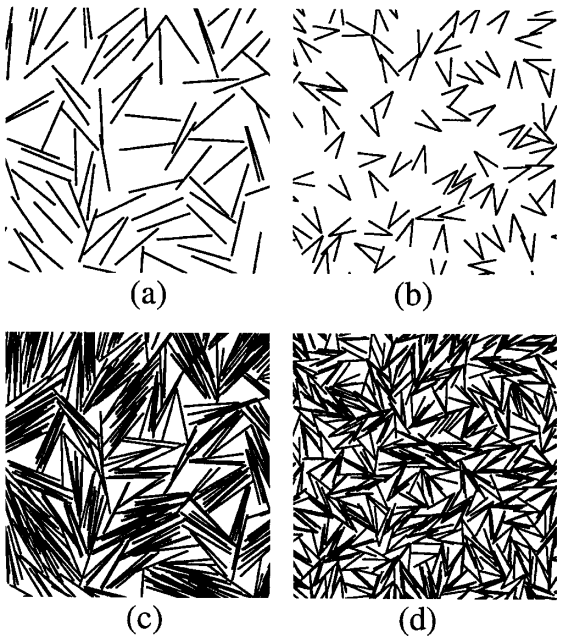

FIG. 3. Snapshots of patterns formed during the RSA of needles ($\phi = 180°$) [(a) and (c)], and the angled objects ($\phi = 30°$) [(b) and (d)]. Total length of the angled object is the same as that of the needle and each of these figures shows the central $\frac{1}{4}$ substrate area. (a) and (b) correspond to the state when 300 objects of each type are adsorbed on the whole substrate, while (c) and (d) correspond to the evolved states of the same portion when 2000 objects of each type are adsorbed on the whole substrate.

they are needles or angled objects. While explaining the slowing down of the adsorption rate in the case of elliptical objects compared to the circular ones, Talbot *et al.* [5] have offered qualitatively similar reasoning, where they observed that unlike for the circular objects, only certain orientations are allowed for ellipses falling in the isolated selective target spaces. Such a different object view is the cause of the more severe limitation on the size of domains in the case of angled objects as compared to those in the case of needles. If one examines the evolution of RSA from Fig. 3(a) to Fig. 3(c) in the case of needles and from Fig. 3(b) to Fig. 3(d) in the case of angled objects, it can be noticed that growth of domains precipitated during early growth is well evolved for the case of needles but is substantially frustrated in the case of angled objects. This is reflected in the relatively low local packing of nearly parallel adsorbed objects in the vicinity of a given object in the case of angled objects as compared to the needles, resulting in a smaller value of the exponent α in the former case.

In the light of above analysis, it is now useful to explore the possible reason for the small but gradual increase of α with an increase of ϕ from $\sim 30°$ to $\sim 150°$ for the angled objects. We refer to the sketches in Fig. 4. Consider a single object already adsorbed. Let us choose the pole O at its vertex, and the polar axis along one of its arms. Let us consider a successful addition taking place with vertex at $A(r, \theta)$ in the vicinity (here by vicinity we mean $r < l$) of the reference object. Each new addition can loosely be classified into either favoring [such as in Fig. 4(a)] or nonfavoring [such as in Fig. 4(b)] further domain growth. A connection with the filling process can be established by considering probabilities of the situations such as those in Figs. 4(a) and 4(b) being generated in an RSA process which we do by geometrical analysis.

Consider a reference object POQ. (See Fig. 5.) Now, for a new object falling in the circle of vicinity, the probability "s" that its vertex lies in the area element $r\,dr\,d\theta$ around $A(r, \theta)$ is given by $s = (r\,dr\,d\theta/\pi l^2)$. For a new object falling at $A(r, \theta)$, selection of a particular orientation could now lead to any of the three possible events: (1) it gets adsorbed and favors domain growth, (2) it gets adsorbed but does not favor domain growth, and (3) it does not get adsorbed because of the overlap with the reference object. In the following analysis, we analyze the events (1) and (2) for their relative strengths as a function of the object angle ϕ. The third case is rejected anyway. Let R_1 and R_2 denote the ranges of orientations corresponding to events (1) and (2), respectively, and let $p_\phi(r, \theta)$ and $q_\phi(r, \theta)$ be the corresponding probabilities given by $p_\phi(r, \theta) = sR_1/(R_1 + R_2)$ and $q_\phi(r, \theta) = sR_2/(R_1 + R_2)$, where R_1 and R_2 are functions of r and θ.

For a typical situation such as that in Fig. 5(a), AP' and AQ' are the limiting positions for the arms of new object. Thus,

$$R_1 = (\psi_1 + \psi_2 - \phi), \qquad \text{if } \psi_1 + \psi_2 \geq \phi \quad \text{and} \quad R_1 = 0 \text{ otherwise},$$

$$R_2 = \phi - (2\pi - \psi_1 - \psi_2), \qquad \text{if } \phi \geq (2\pi - \psi_1 - \psi_2) \quad \text{and} \quad R_2 = 0 \text{ otherwise},$$

where $\psi_1 = \sin^{-1}[r \sin(\theta)/l] + \theta$ and $\psi_2 = \sin^{-1}[r \sin(\phi - \theta)/l] + (\phi - \theta)$. One more typical possibility among many others is shown in Fig. 5(b). Here

$$R_1 = \phi - (2\pi - \psi), \qquad \text{if } \phi \geq (2\pi - \psi) \quad \text{and} \quad R_1 = 0 \text{ otherwise},$$

$$R_2 = \psi - \phi, \qquad \text{if } \psi \geq \phi \quad \text{and} \quad R_2 = 0 \text{ otherwise},$$

where $\psi = \sin^{-1}[r \sin(\theta - \phi)/l] + (\theta - \phi) + \pi$.

By considering all the possible cases carefully, the values of the total probabilities of domain favoring and nonfavoring adsorption in the vicinity, namely P_ϕ and Q_ϕ, respectively, are obtained by numerically integrating over the whole range of $r(0 \leq r \leq l)$ and $\theta(0 \leq \theta \leq 2\pi)$. In Fig. 6 we plot the probability ratio m_ϕ defined as $m_\phi = P_\phi/Q_\phi$, which gives the relative strength of domain favoring and nonfavoring adsorption, as a function of $\phi(30° \leq \phi \leq 150°)$. Interestingly, the value of m_ϕ increases

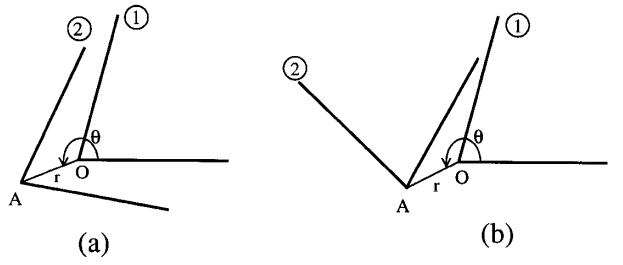

FIG. 4. (a) Relative positions of objects (1) and (2) which favor domain growth. (b) Relative positions of objects (1) and (2) which do not favor domain growth.

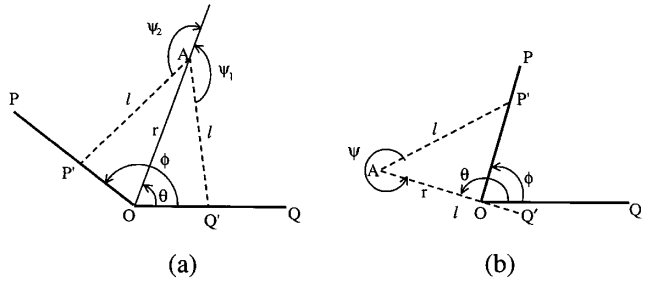

FIG. 5. (a),(b) Illustrations regarding the calculations of the probabilities $p_\phi(r, \theta)$ and $q_\phi(r, \theta)$.

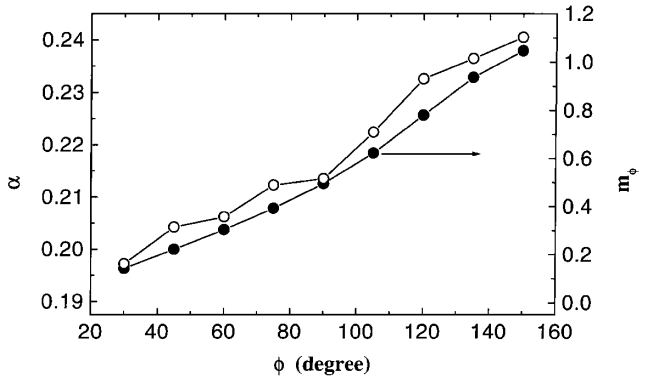

FIG. 6. Exponent α and the measure m_ϕ both plotted against object angle ϕ for $30° \leq \phi \leq 150°$. The arrow indicates that m_ϕ values refer to the right axis.

gradually with ϕ. Thus, for objects with higher values of ϕ, there is reduction in the overall interdomain space, which results in a higher value of exponent α. Also shown in Fig. 6 is the exponent α plotted against ϕ. Remarkably, m_ϕ and α have similar trends.

We now seek a connection between α and m_ϕ. We first recognize that for line segments the relationship $\rho(t) \propto t^{\alpha'}$ has been established, where $\alpha' = \sqrt{2} - 1$ is obtained analytically [9] and 0.38 from simulations [8]. This implies that the probability of adsorption of a line segment to occur between time t and $t + dt$, which is proportional to $d\rho/dt$ is given by $A\rho^{(\alpha'-1)/\alpha'}$. We now look at the deposition of the angled object with object angle ϕ as simultaneous connected deposition of two line segments, and therefore the probability for such adsorption should multiply two probability expressions for line segments, with an added qualification for the angle dependent quality of adsorption space represented by m_ϕ. Thus for angled objects, we can write

$$d\rho/dt = C\{\rho^{(\alpha'-1)/\alpha'-\varepsilon(\phi)}\}^2.$$

Here $\varepsilon(\phi)$ is a positive real number which represents the ϕ-dependent segment connectivity and adsorption space qualification related to m_ϕ. Since small m_ϕ stands for less domain favoring situation, it must lead to smaller $d\rho/dt$, and hence to a higher value of $\varepsilon(\phi)$.

We point out that the current analysis using an analytic expression of the form $d\rho/dt \propto \{\rho^{(\alpha'-1)/\alpha'-\varepsilon(\phi)}\}^2$ does not embody the nonanalytic discontinuities in the exponent at $\phi = 0°$ or 180°. The discontinuities originate from the fact that even an infinitesimally small departure of the angle from 0° or 180° changes the dependence itself from $\rho^{(\alpha'-1)/\alpha'}$ to $\{\rho^{(\alpha'-1)/\alpha'-\varepsilon(\phi)}\}^2$.

Reorganizing, and integrating, we get

$$\rho = [C(1 - k)t]^{1/(1-k)},$$

where $k = 2(\alpha' - 1)/\alpha' - 2\varepsilon(\phi)$. Thus, for angled objects, we can write $\rho \propto t^\alpha$ for the object angles away from the crossover regions; α being given by

$$\alpha = 1/(1 - k) = \alpha'/[2 - \alpha' + 2\alpha'\varepsilon(\phi)].$$

Note that when $\varepsilon(\phi)$ is very small, such as for object angles close to 150° [where one is not in the crossover regime, yet the object is almost linear and the perturbation $\varepsilon(\phi)$ is expected to be small], $\alpha \sim 0.26$. Interestingly, it matches extremely well with our simulation value of ~0.25 obtained for the object angles close to 150°. Estimating $\varepsilon(\phi)$ values from $\alpha = \alpha'/[2 - \alpha' + 2\alpha'\varepsilon(\phi)]$ by using $\alpha' = (\sqrt{2} - 1)$ and the values of α obtained from simulations, we find a linear relation between $\varepsilon(\phi)$ and m_ϕ of the form $\varepsilon(\phi) = -0.5m_\phi + 0.65$.

In conclusion, we have carried out RSA simulation of zero-area objects with different shapes, namely the needles and the symmetric angled objects with a wide range of angles between the arms. The value of the exponent α [in $\rho(t) \sim t^\alpha$, where $\rho(t)$ is the number density] exhibits a crossover near $\phi = 0°$ or 180°, and is significantly lower in the case of the angled objects as compared to that in the case of needles. This establishes the crucial role of the geometrical character of the zero-area object in RSA dynamics, and the corresponding contribution to the value of the exponent α. This work also highlights the significance of interdomain space in the dynamics of RSA.

One of the authors (M. D. K.) gratefully acknowledges CSIR (Government of India) for the financial support.

*Electronic address: mdk@physics.unipune.ernet.in
†Electronic address: avl@physics.unipune.ernet.in
‡Electronic address: ogale@squid.umd.edu

[1] J. W. Evans, Rev. Mod. Phys. **65**, 1281 (1993); B. Bonnier, M. Hontebeyrie, Y. Leroyer, C. Meyer, and E. Pommiers, Phys. Rev. E **49**, 305 (1994); J-S. Wang and R. B. Pandey, Phys. Rev. Lett. **77**, 1773 (1996); V. Privman, J-S. Wang, and P. Nielaba, Phys. Rev. B **43**, 3366 (1991); G. Y. Onoda and E. G. Liniger, Phys. Rev. A **33**, 715 (1986).
[2] R. H. Swendsen, Phys. Rev. A **24**, 504 (1981).
[3] J. Feder, J. Theor. Biol **87**, 237 (1980).
[4] G. Tarjus and P. Viot, Europhys. Lett. **13**, 295 (1990).
[5] J. Talbot, G. Tarjus, and P. Schaaf, Phys. Rev. A **40**, 4808 (1989).
[6] P. Viot, G. Tarjus, S. M. Ricci, and J. Talbot, Physica (Amsterdam) **191A**, 248 (1992).
[7] J. D. Sherwood, J. Phys. A **23**, 2827 (1990).
[8] R. M. Ziff and R. D. Vigil, J. Phys. A **23**, 5103 (1990).
[9] G. Tarjus and P. Viot, Phys. Rev. Lett. **67**, 1875 (1991).
[10] R. D. Vigil and R. M. Ziff, J. Chem. Phys. **91**, 2599 (1989); **93**, 8270 (1990).